Mon. Not. R. Astron. Soc. **000**, 000–000 (0000) Printed 2 February 2008 (MN LATEX style file v2.2)

The intergalactic medium temperature and Compton y parameter

Pengjie Zhang⋆, [1]† Ue-Li Pen, [2]‡ Hy Trac, [2],[3]§
1*NASA/Fermilab Astrophysics Group, Fermi National Accelerator Laboratory, Box 500, Batavia, IL 60510-050*
2*Canadian Institute for Theoretical Astrophysics, University of Toronto, Toronto, Canada, M5S 3H8*
3*Department of Astronomy & Astrophysics, University of Toronto, Toronto, Canada, M5S 3H8*

2 February 2008

ABSTRACT
The thermal Sunyaev Zeldovich (SZ) effect directly probes the thermal energy of the universe. Its precision modeling and future high accuracy measurements will provide a powerful way to constrain the thermal history of the universe. In this paper, we focus on the precision modeling of the gas density weighted temperature $\bar{T}_g$ and the mean SZ Compton y parameter. We run high resolution adiabatic hydro simulations adopting the WMAP cosmology to study the intergalactic medium (IGM) temperature and density distribution. To quantify possible simulation limitations, we run $n = -1,-2$ self similar simulations. Our analytical model on $\bar{T}_g$ is based on energy conservation and matter clustering and has no free parameter. Combining both simulations and analytical models thus provides the precision modeling of $\bar{T}_g$ and $\bar{y}$. We find that the simulated temperature probability distribution function and $\bar{T}_g$ shows good convergence. For the WMAP cosmology, our highest resolution simulation (1024^3 cells, 100 Mpc/h box size) reliably simulates $\bar{T}_g$ with better than 10% accuracy for $z \gtrsim 0.5$. Toward $z = 0$, the simulation mass resolution effect becomes stronger and causes the simulated $\bar{T}_g$ to be slightly underestimated (At $z = 0$, $\sim 20\%$ underestimated). Since $\bar{y}$ is mainly contributed by IGM at $z \gtrsim 0.5$, such simulation effect on $\bar{y}$ is no larger than $\sim 10\%$. Furthermore, our analytical model is capable of correcting this artifact. It passes all tests of self similar simulations and WMAP simulations and is able to predict $\bar{T}_g$ and $\bar{y}$ to several percent accuracy. For low matter density ΛCDM cosmology, the present $\bar{T}_g$ is $0.32(\sigma_8/0.84)^{3.05-0.15\Omega_m}(\Omega_m/0.268)^{1.28-0.2\sigma_8}$ keV, which accounts for 10^{-8} of the critical cosmological density and 0.024% of the CMB energy. The mean y parameter is $2.6\times10^{-6}(\sigma_8/0.84)^{4.1-2\Omega_m}(\Omega_m/0.268)^{1.28-0.2\sigma_8}$. The current upper limit of $y < 1.5\times10^{-5}$ measured by FIRAS has already ruled out combinations of high $\sigma_8 \gtrsim 1.1$ and high $\Omega_m \gtrsim 0.5$.

Key words: Cosmic microwave background-theory-simulation: large scale structure, intergalactic medium, intracluster gas, cosmology, thermal history

1 INTRODUCTION

Ionized electrons with thermal motion can scatter CMB photons to generate secondary CMB temperature fluctuations known as the thermal Sunyaev Zeldovich (SZ) effect. Since all free electrons participate in the inverse Compton scattering and contribute to the SZ effect, the SZ effect is an unbiased probe of the thermal energy of the universe at $z \lesssim 6$, for which the universe is highly ionized. The thermal SZ effect is sensitive to various physical processes like adiabatic gravitational heating, feedback, preheating and radiative cooling (da Silva et al. 2001; Lin et al. 2002; White, Hernquist & Spingel 2002; Zhang & Wu 2003) which affect the thermal energy of the baryons. In addition, Compton cooling of first star supernova remnants (Oh, Cooray & Kamionkowski 2003), cluster magnetic field (Zhang 2004), etc. could further alter the thermal energy of the universe to the level of $\gtrsim 10\%$. Therefore, the precision measurement and interpretation are of great importance to understand the thermal history of the universe.

Current CMB experiments such as CBI(Bond et al. 2002; Mason et al. 2003), BIMA(Dawson et al. 2002) and ACBAR (Kuo et al. 2002) marginally detected the SZ effect. Several upcoming CMB experiments such as ACT,

† E-mail:zhangpj@fnal.gov
‡ E-mail:pen@cita.utoronto.ca
§ E-mail:trac@cita.utoronto.ca

APEX, Planck, SPT and SZA are likely able to measure the SZ effect with $\sim 1\%$ accuracy in the next several years. In order to utilize the power of such accurate experiments, the modeling of the SZ effect is required to meet this $\sim 1\%$ accuracy. The first natural step for such modeling is to robustly understand the evolution of the baryon thermal energy in an adiabatically evolving universe. It is not only required to extract more complicated physics by comparing with observations but also provides clues for the modeling of these complicated physics.

Much effort has been devoted toward this goal, both analytically (Cole & Kaiser 1988; Makino & Suto 1993; Atrio-Barandela & Mucket 1999; Komatsu & Kitayama 1999; Cooray, Hu & Tegmark 2000; Molnar & Birkinshaw 2000; Majumdar 2001; Zhang & Pen 2001; Komatsu & Seljak 2002) and simulationally (da Silva et al. 2000; Refregier et al. 2000; Seljak, Burwell & Pen 2001; Springel, White & Hernquist 2001; Zhang, Pen & Wang 2002). Both methods have limitations, which has not been quantified and corrected to meet the precision of future observations. Analytical models of the SZ effect are often *ad hoc* procedures. In the halo model, the cluster gas pressure distribution is a free function of cluster mass and redshift. Though it can be calculated by various assumptions such as hydrostatic equilibrium, its uncertainty is hard to quantify. In the continuum field model (Zhang & Pen 2001), the gas temperature is determined by the gravitational potential, whose zero point is determined somewhat arbitrarily. So, analytical models must be tested and calibrated against simulations. For instance, Refregier & Teyssier (2002) has tested the halo model against simulations and found good agreement. However, the conclusions drawn from these comparisons should be viewed with some caution. Numerical simulations are known to have artifacts, stemming from limited resolution and finite volume. The impact of some of the artifacts have been investigated for the thermal SZ effect (Refregier & Teyssier 2002) and the kinetic SZ effect (Zhang, Pen & Trac 2004). If not corrected, such artifacts would lead to biased calibrated analytical models.

The SZ mean temperature decrement, or equivalently, the mean SZ Compton y parameter, which corresponds to the density weighted gas mean temperature $\bar{T}_g$, are the lowest order SZ statistics. They are also the easiest to simulate and model. So, the precision prediction of $\bar{T}_g$ and $\bar{y}$ stands as the first natural step toward the precision modeling of the SZ effect. Their precision modeling also provides clues for the next low order SZ statistics such as the SZ power spectrum and the corresponding gas pressure power spectrum. In this paper, we present a detailed study of the IGM density and temperature distribution from a series of ΛCDM and self similar simulations. We further test the continuum model prediction of $\bar{T}_g$ and y parameter against simulations. Our goal is to quantify and correct numerical limitations and build calibrated analytical model aimed at 1% accuracy. We will follow a similar procedure as in this paper to discuss the precision modeling of the SZ power spectrum in a companion paper (Zhang, Pen & Trac, 2004, in preparation).

2 THE THERMAL SUNYAEV-ZELDOVICH EFFECT

Free electrons scatter off CMB photons by their thermal motions and introduce secondary CMB temperature fluctuations:

$$\Theta = -2yS_T(\nu) = -2y\left[2 - \frac{x/2}{\tanh(x/2)}\right], \quad (1)$$

where $x \equiv h\nu/k_BT_{\rm CMB}$. This is known as the thermal Sunyaev-Zeldovich (SZ) effect (Zeldovich & Sunyaev 1969). The Compton y parameter is given by the integral of electron thermal pressure energy along the line of sight

$$y = \int \frac{n_e k_B T_e}{m_e c^2}\sigma_T a d\chi, \quad (2)$$

where χ is the comoving distance and a is the scale factor. The lowest order statistics of the SZ effect is the mean Compton y parameter:

$$\bar{y} = -2.37\times10^{-4}\Omega_b h\int \frac{\bar{T}_g}{\rm keV}a^{-2}d\tilde{\chi}, \quad (3)$$

where $\bar{T}_g \equiv \langle(1+\delta_g)T_g\rangle$ is the gas density weighted mean temperature and $\tilde{\chi} \equiv \chi/(c/H_0)$ is the dimensionless comoving distance while H_0 is the present Hubble constant.

The thermal energy of the universe only accounts for a tiny fraction of the total energy of the universe.

$$\Omega_{\rm TE} = 1.08\times10^{-8}\frac{\bar{T}_g}{0.3{\rm keV}}\frac{\Omega_b h^2}{0.02}\ . \quad (4)$$

As a comparison, $\Omega_{\rm CMB} = 2.48\times10^{-5}h^{-2}$ and the energy in other wavelength bands of light

$$\Omega_{\rm EBL} = 2.48\times10^{-6}h^{-2}\frac{I_{\rm EBL}}{100\ {\rm nw\ m^{-2}\ sr^{-1}}}\ . \quad (5)$$

3 HYDRO SIMULATIONS

We ran cosmological hydrodynamical simulations using a new Eulerian cosmological hydro code (Trac & Pen 2003a,b). This Eulerian code (hereafter TP) is based on the finite-volume, flux-conservative total variation diminishing (TVD) scheme that provides high-order accuracy and high-resolution capturing of shocks. The hydrodynamics of the gas is simulated by solving the Euler system of conservation equations for mass, momentum, and energy on a fixed Cartesian grid. The gravitational evolution of the dark matter is simulated using a cloud-in-cell particle-mesh (PM) scheme (Hockney & Eastwood 1988).

The robustness of the TP code has been tested by comparing the evolution of the dark matter and gas density power spectra from the simulations with the fitting formula of Smith et al. (2003). We also performed a code comparison by running the same initial conditions using the MMH code (Pen 1998), which combines the shock capturing abilities of Eulerian schemes with the high dynamic range in density achieved by Lagrangian schemes. Power spectra are computed using FFTs. We find good agreement at all relevant scales and redshifts for both comparisons.

Eulerian schemes are ideal for simulating the evolution of the IGM to model the thermal and kinetic SZ effects and

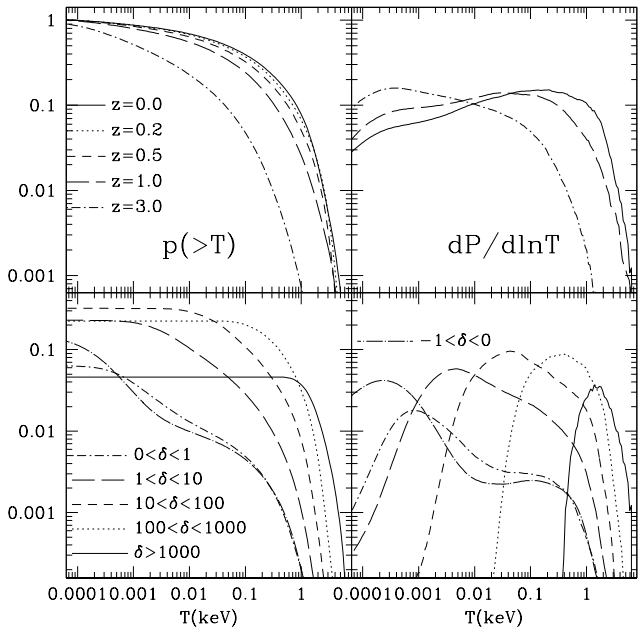

Figure 1. The gas temperature distribution in the 1024^3, 100 Mpc/h WMAP simulation. The top left panel shows the cumulative mass fraction $p(>T)$ with temperature higher than T. The bottom bottom panel shows the conditional $p(>T)$ in different overdensity regions at $z = 0$. The right panels plot the corresponding $\mathrm{d}P/\mathrm{d}\ln T$. At $z = 0.0$, only 5% gas is hotter than 1 keV. Gas temperature is tightly correlated with gas density. Nearly all virialized gas is hotter than 1 keV while effectively no gas with $\delta < 10$ is hotter than 0.1 keV.

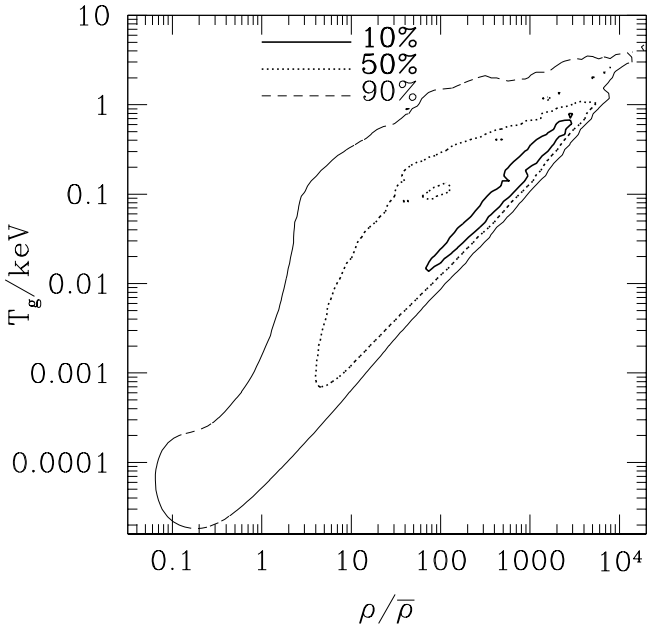

Figure 2. The contour of gas (log)temperature and (log)density in the 1024^3 WMAP simulation. Gas temperature strongly correlates with gas density with a scaling relation $T \propto \rho$, as found in previous works (e.g. Kang et al. (1994); Dave et al. (2001)).

the Lyman alpha forest, because of their high speed, superior mass resolution, shock-capturing abilities. Furthermore, Eulerian algorithms are computationally very fast and memory friendly, allowing one to optimally use available computational resources.

We ran a 1024^3 cells, 100 Mpc/h box size simulation with the best fit WMAP-alone cosmology $\Omega_m = 0.268$, $\Omega_\Lambda = 0.752$, $\Omega_b = 0.044$, $h = 0.71$, and $\sigma_8 = 0.84$ (Spergel et al. 2003). The ratio of dark matter particles to fluid elements is 1:8. We achieve a spacial resolution of $\Delta x \simeq 100$ kpc/h and a dark matter particle mass resolution of $\Delta m \simeq 5.6 \times 10^8\ M_\odot$. The initial conditions are generated by sampling from an initial power spectrum computed using CMBFAST (Seljak & Zaldarriaga 1996). This simulation is started at a redshift of $z = 100$ and evolved down to $z = 0$, with data outputs at $z = 3$, 1, 0.5, 0.2 and 1. This simulation takes approximately 700 time-steps to evolve from $z = 100$ down to $z = 0$. On a GS320 Compaq Alpha server with 32 cpus and total theoretical peak speed of 32 Gflops, the run **requires 40 G memeory** and takes approximately two days. Simulations are limited by both the box size, which causes the absence of large scale density fluctuation at scales larger than half box size, and resolution, which results in the failure to resolve small scale structures. Self similar simulations are ideal to test and quantify such simulation limitations since different redshifts directly corresponds to different resolution and box size. We ran one $n = -2$ and one $n = -1$ ($\Omega_m = 1$) self similar simulation with 512^3 cells and the same amount of dark matter particles. In these simulations, Ω_b is set to be 0.044/0.268 to mimic the Ω_b/Ω_m ratio of the WMAP cosmology. The initial fluctuation is normalized such that, when linearly extrapolated to $z = 0$, the correlation length is half the simulation box size. We also run a 512^3 cells, 100 Mpc/h WMAP simulation with the identical initial condition as the 1024^3 for a direct comparison. The moving frame of the TP code is not turned on in these runs. We will check its effect in the future.

We show the temperature distribution function, namely the mass fraction of gas hotter than T, $p(>T)$ of the 1024^3 WMAP simulation in Fig. 1. At $z = 0.0$, only 5% gas are hotter than 1 keV and $\sim 40\%$ gas are hotter than 0.1 keV. These fraction drops to 3% and 24% at $z = 1.0$. Gas temperature shows a strong positive correlation with its density. At $z = 0.0$, nearly all gas with $\delta \gtrsim 1000$ are hotter than 1 keV. For $100 < \delta < 1000$, almost all gas are hotter than 0.1 keV. Nearly no gas hotter than 0.1 keV lies in $\delta < 10$ region. It is interesting to see how much gas lies in virialized halos. Virialized gas should have an overdensity larger than that of the gas overdensity at the virial radius. For an isothermal density profile $\rho \propto r^{-2}$, this states $\delta \geqslant \delta(r_{\rm vir}) = 1/3\Delta_c/\Omega_m \sim 100$. $\Delta_c \sim 100$ for WMAP (Eke et al. 1996) is the mean matter density in a virialized halo with respect to the critical density. This factor 1/3 does not change much for other profiles such as NFW and thus we omit its variation. Then the bottom panel of Fig. 1 implies that only $\sim 28\%$ gas resides in virialized halos. At $z = 1.0$, this fraction drops to $\sim 19\%$.

In our simulation, a large fraction of gas is colder than $\sim 10^4$K. At $z = 0$, this fraction is $\sim 10\%$ and at $z = 3$, this

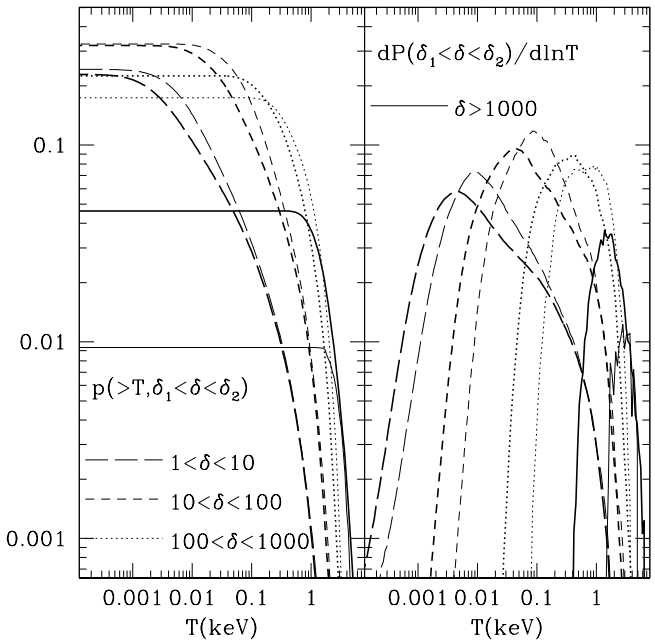

Figure 3. The comparison of the conditional temperature distribution function $p(>T, \delta_1 < \delta < \delta_2)$ between WMAP 1024^3 (thick lines) and 512^3 (thin lines) simulations. For clarity, we only show $\delta > 1000$ (solid lines), $1000 > \delta > 100$ (dot lines), $100 > \delta > 10$ (short dash lines), $10 > \delta > 1$ (long dash lines). Though the overall $p(>T)$ agrees very well for two simulations (Fig. 5), the conditional $p(>T, \delta_1 < \delta < \delta_2)$ does not converge yet and reflects the effect of simulation resolution. $\delta \gtrsim 1000$ corresponds to the inner regions of clusters and groups. For these virialized objects, their temperature scales with respect to their mass M as $M^{2/3}$. For clusters with virial radius around 1 Mpc/h, $T \sim 1$ keV. Higher resolution simulations are able to resolve more low mass halos, which are smaller and have lower T and thus result in a higher $p(>T, \delta > 1000)$ at $T \lesssim 1$ keV. The limited simulation resolution introduces artifacts into the T-ρ correlation. Though its effect to the gas density weighted temperature is minor (Fig. 5), it would affect the simulated pressure power spectrum significantly.

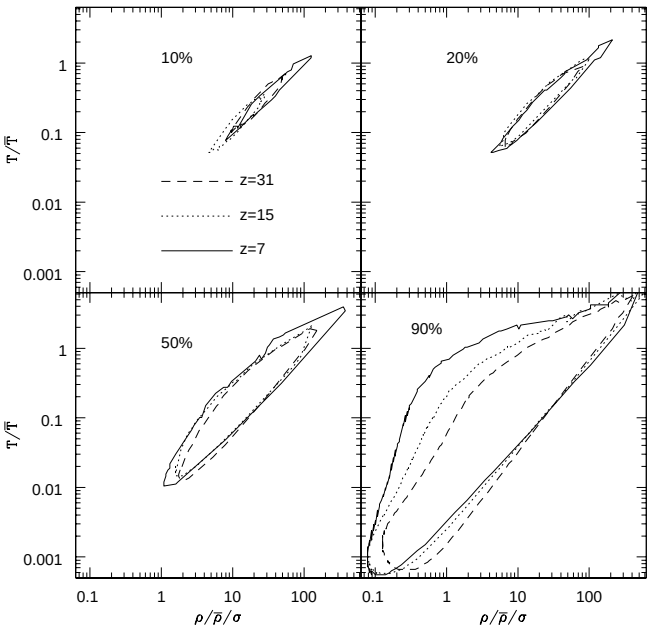

Figure 4. The contour of gas (log)temperature and (log)density in the $n = -1$ self similar simulation. The simulations show good convergence in most T-ρ regions. Higher resolution is required to simulate both low T, low ρ regions and high T, high ρ regions. But low T, low ρ regions have little contribution to mean gas density weighted temperature.

fraction reaches $\sim 50\%$. In reality, part of these gas may condense into stars or interstellar medium. Part of them may be photoionization-heated to above 10^4K. Our simulation does not include any photoionization, radiative cooling, etc., so the prediction about these gas is not reliable and is hard to compare with other works (e.g. Kang et al. (1994); Dave et al. (2001)). But the contribution of such gas to the SZ effect is negligible due to their low temperature, so we omit the complexity caused by such gas.

The strong correlation of T and ρ observed in $p(>T, >\rho)$ is clearly shown in the T-ρ contour of our 1024^3 simulation (Fig. 2). $T \propto \rho$ holds in a large T-ρ regions, as found in previous works (e.g. Kang et al. (1994); Dave et al. (2001)).

Simulations are both mass and spacial resolution limited. So the above results may be strongly resolution dependent. Both the Press-Schechter formalism (Press & Schechter 1974) and the Jenkins fitting formula (Jenkins et al. 2001) imply the existence of numerous small halos. The failure to resolve these small halos will result in an underestimation of the fraction of virialized gas and biased T-ρ relation. To estimate the resolution effect, we compare between WMAP simulations and between self similar simulations.

In low density regions, the density field is well resolved. But such regions generally have high Mach number and thus shocks are relatively poorly resolved. Since gas thermal energy is generated by shock heating, in low density regions, temperature field is likely poorly resolved. In high density regions, it is the opposite case. Fig. 3 shows that both fields are indeed significantly affected by resolutions. The fraction of $\delta > 1000$ gas increases from $\sim 1\%$ in the 512^3 simulation to $\sim 5\%$ at 1024^3. The 1024^3 simulation is able to resolve smaller halos, which have lower temperature and results in an increase in $dp(>T, \delta > 1000)/d\ln T$ at $T \lesssim 3$ keV. The fraction of virialized gas ($\delta \gtrsim 100$) increases from $\sim 18\%$ to $\sim 28\%$. For $\delta < 10$, the conditional $p(>T)$ agrees well at the high T tail where Mach numbers are low and diverges at the low T tail where Mach numbers are high. So, for $\delta < 10$, shock capture is the dominant resolution factor. In summary, the IGM density and temperature distribution in simulations is mainly limited by density resolution in high density regions and shock capturing ability in low density regions. We thus expect that higher resolution simulations will result in larger dispersion in the gas ρ-T phase space distribution, and thus larger pressure dispersion. This conclusion is further confirmed in the T-ρ contours of the probability distribution for our self similar simulation results (Fig. 4). Such resolution effect has only minor effect on $\bar{T}$, but its effect on the pressure power spectrum may be important. We will study this issue in a companion paper (Zhang, Pen & Trac, 2004, in preparation).

Our simulations suggest that (1) only a small

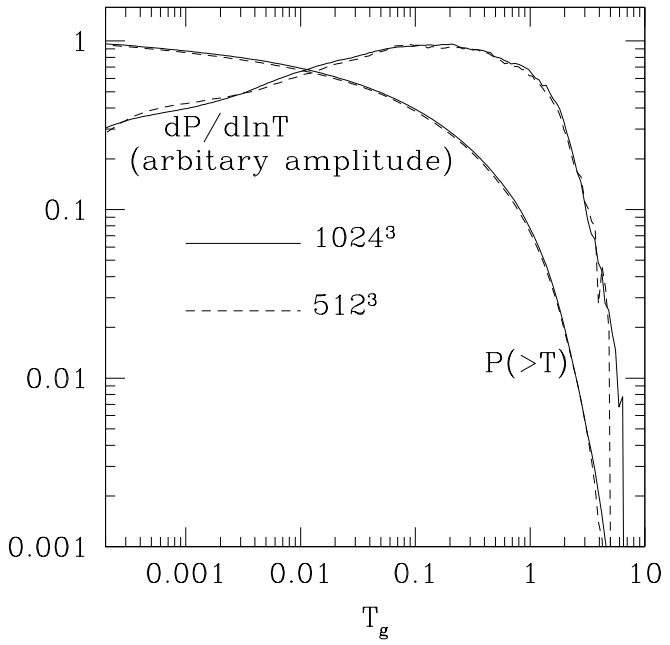

Figure 5. The comparison of the overall temperature distribution function $p(>T)$ between the WMAP 1024^3 and the 512^3 simulations. Two simulations agree well. $p(>T)$ is directly related to the mean gas mass weighted temperature $\bar{T}_g$ through the relation $\bar{T}_g \equiv \int T\mathrm{d}p$. The good convergence of $p(>T)$ implies that the simulation effects to $\bar{T}_g$ is minor, though we will still quantify them in §4.

fraction of gas are virialized and (2) a strong correlation exists between gas temperature and density. Both apparently contradict with the halo model. The halo model assumes that all gas resides in virialized halos. This assumption seems to contradict with (1), as noticed by Refregier & Teyssier (2002). The simplest version of the halo model assumes gas to be isothermal with temperature equal to its virial temperature. Since halos roughly have the same density, the predicted T-ρ correlation should be very weak. The weak dependence of halo concentration number on halo mass can not alter this straight prediction. More complicated intracluster gas models such as the *universal gas profile* (Komatsu & Seljak 2001) predict a weak variation of gas temperature from the core to the virial radius. But such variation is still too weak to explain the simulated $T \propto \rho$ relation.

But simulations are resolution limited and some artifacts can be clearly seen in Fig. 3. It is likely that the part of the contradictions discussed above are caused by the limited simulation resolution. The limited simulation resolution effectively smooths the density field and may cause an underestimation of the fraction of virialized gas. The spacial resolution (~ 0.1 Mpc/h for our largest simulation) instead of the mass resolution is the main limiting factor to resolve halos. If our simulation only resolves halos with virial radius $r_{\rm vir} \geqslant r_{\rm min} \sim 0.5$ Mpc/h, following the Press-Schechter formalism (Press & Schechter 1974), such halos contain $f_h = 1 - \mathrm{Erf}[-\nu/\sqrt{2}] \sim 30\%$ of the total mass at $z = 0$. Here, $\nu \equiv \delta_c/\sigma(m_{\rm min})$, where $\delta_c \sim 1.686$ is the density threshold, $\sigma(m)$ is the density fluctuation in a sphere with mean mass m and $m_{\rm min}$ is the mass of halos with $r_{\rm vir} = r_{\rm min}$. This mass fraction is consistent with our simulation results. But this predicted mass fraction is very sensitive to the $r_{\rm min}$ assumed. For example, if $r_{\rm min} \sim 0.3$ Mpc/h, the predicted virialized gas fraction would be $f_h \sim 50\%$ and thus contradicts with our simulation result. One can also compare the prediction of $p(>T)$ of halo model with our simulation. The gas temperature T of a halo mass m can be estimated by $T = T_8(m/m_8)^{2/3}$, where at $z = 0$, $T_8 \sim 5\Omega_m \simeq 1.3$ keV (Pen 1998) and m_8 is the mean mass contained in a sphere with radius 8 Mpc/h. Thus the halo model predicts $p(\gtrsim 1.3\mathrm{keV}) = f_h(m \geqslant m_8) \sim 4\%$, and $p(\gtrsim 0.1\mathrm{keV}) \simeq f_h(m \geqslant 0.02m_8) \sim 50\%$. These predictions are roughly consistent with our simulation result. Thus, a low fraction of virialized gas may be caused by simulation resolution.

The effect of resolution to the $\rho - T$ relation can be estimated as follow.[1]. The density profile of each halo can be approximated as $\delta = \delta_{\rm vir}(r/r_{\rm vir} \sim 100(r/r_{\rm vir})$. The smoothing caused by limited resolution convolves this density field with a window function with radius R_f. For halos with $r_{\rm vir} \lesssim R_f$, the smoothed density δ^f will be $\delta^f \sim 100(r_{\rm vir}/R_f)^2 \propto T$. Here, we have utilized that $r_{\rm vir} \propto M^{1/3} \propto T^{1/2}$. For WMAP cosmology at $z = 0$, this implies that $\delta \sim 100(1\mathrm{Mpc/h}/R_f)^2(T/\mathrm{keV})$. This relation is surprisingly consistent with our simulation, if taking $R_f \simeq 0.2$ Mpc/h. So the $\rho - T$ relation may also be caused by artifacts of simulations and has to be used in caution.

On the other hand, the simulation resolution is hard to explain all aspects of simulation results. The ρ-T relation shows a robust convergence in the self similar simulations (e.g. 20%, 50% ρ-T contour in Fig. 4) and only changes very slowly as the nonlinear length scale changes by a factor of 4. This suggests that it is unlikely that the observed ρ-T relation is purely caused by simulation artifacts, otherwise the ρ-T relation would change significantly with resolution.

These issues deserves further investigations. But more careful comparison requires more realistic halo mass function than the Press-Schechter formalism and a series of simulations to have fair sample of $\sim$ keV halos and thus beyonds the scope of this paper.

But despite these significant resolution effects on both density and temperature fields, the simulated overall $p(>T)$ shows a good convergence except at very low or high temperature ranges (Fig. 5 & 6). Since the energy conservation guarantees the total amount of kinetic and thermal energy to be well simulated, the good agreement of $p(>T)$ implies that the conversion efficiency from kinetic energy to thermal energy is well simulated too. Since $\bar{T}_g \equiv \int T dp$, the effect

[1] The discussion presented here is based on the comments of the anonymous referee.

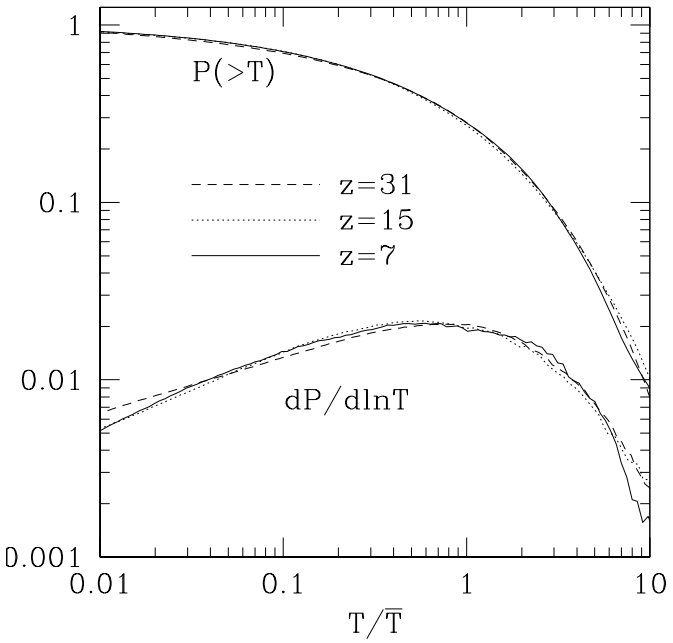

Figure 6. The overall temperature distribution $p(> T)$ for $n = -1$ self similar simulation. For the temperature field, the simulation effect is minor except for very low or high temperature regions. Since the gas density weighted temperature $\bar{T}_g = \int T dp$, $\bar{T}_g$ is well simulated.

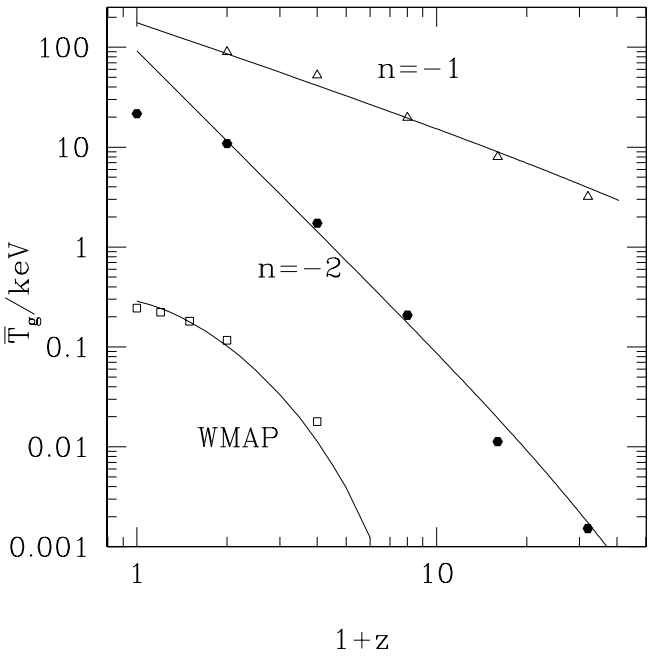

Figure 7. The density weighted gas temperature $\bar{T}_g$. Data points are the results of our self similar simulations (512^3), WMAP simulation (1024^3, 100 Mpc/h) and solid lines are our model predictions. Our model predicts a self similar scaling relation $\bar{T}_g(z) \propto (1+z)^{(n-1)/(n+3)}$ for self similar simulations. Our predictions agree with simulations very well at most redshifts. The breaking of the self similar relation at low redshifts suggests the limitation of simulations. We will show that the discrepancy of the WMAP simulation at low redshifts is caused by simulation resolution in fig. 8 while the discrepancy of the self similar simulations is caused by limited box size.

of simulation limitations to $\bar{T}_g$ should be minor, as we will quantify in the next section.

The simulated $\bar{T}_g(z)$ would be less resolution dependent and robust. We will develop our model for $\bar{T}_g(z)$ in the next section, test it against simulations, quantify simulation artifacts and provide a precision model of $\bar{T}_g(z)$. As we will show in §4, the simulation effect on $\bar{T}_g$ is only non-negligible at $z \lesssim 0.5$ and this effect is no bigger than $\sim 20\%$, even at $z = 0$.

4 THE CONTINUUM FIELD MODEL

In a gravitational heating scenario, the gas temperature is determined by the gravitational potential Φ. The pressure depends on the thermalized fraction of the total kinetic energy. The translational kinetic energy is thermalized from the energy released when particles shell cross. A model of the thermalized energy is thus given by the difference in energy between two particles separated by a non-linear scale in Lagrangian space, which is the distance at which they can be expected to have shell crossed. The exact procedure amounts to solving the non-linear evolution equations directly. But we can treat the effect statistically in a linear fashion. In the initial linear evolution, the gravitational potential remains constant. After virialization, the gravitational energy at a fixed location remains almost constant. In an Eulerian description, we can describe the energy of particles at a final virialized location as the energy released as a particle travels from its initial position to the final virialized location. We can then relate the gas temperature to Φ through the viral theorem:

$$k_B T_g(\mathbf{x}) = \frac{1}{6}\frac{4m_H}{3+5X}\left[\Phi(\mathbf{x}) - \bar{\Phi}(\mathbf{x})\right]. \quad (6)$$

Since the initial position is not exactly known, we take a spherical average over the non-linear scale to average over all possible initial locations and obtain the mean initial potential

$$\bar{\Phi}(\mathbf{x}) = \int \Phi(\mathbf{x}')W_e(\mathbf{x}-\mathbf{x}')d^3x'. \quad (7)$$

For a detailed explanation, refer to Zhang & Pen (2001). Then, the averaged gas density weighted temperature

$$\bar{T}_g = 0.016\Omega_m \mathrm{keV}(1+z)\int_0^\infty \Delta^2_{\rm dg}(k) f_e(k)\frac{dk}{k}. \quad (8)$$

Here, $f_e(k) \equiv [1 - W_e(k)]/k^2$ (k is in unit of Mpc/h). $\Delta^2_{\rm dg}$ is the dark matter-gas cross correlation power spectrum.

In our model, $W_e(k)$ is a free function, but its asymptotic behavior toward $k = 0$ is fixed by the requirement that T_g follows the density field at large scales, or equivalently, the T_g bias with respect to the underlying density field is a constant at large scales. Its behavior at small scales is hard to determine from first principles. But since at scales smaller than smoothing scale, $W_e(k) \to 0$ and $f_e(k) \to k^{-2}$, the exact behavior of $W_e(k)$ at large k is not very important. Based on these considerations, a natural choice of $W_e(k)$ is a Gaussian function $W_e(k) = \exp(-k^2 r_e^2)$. For this func-

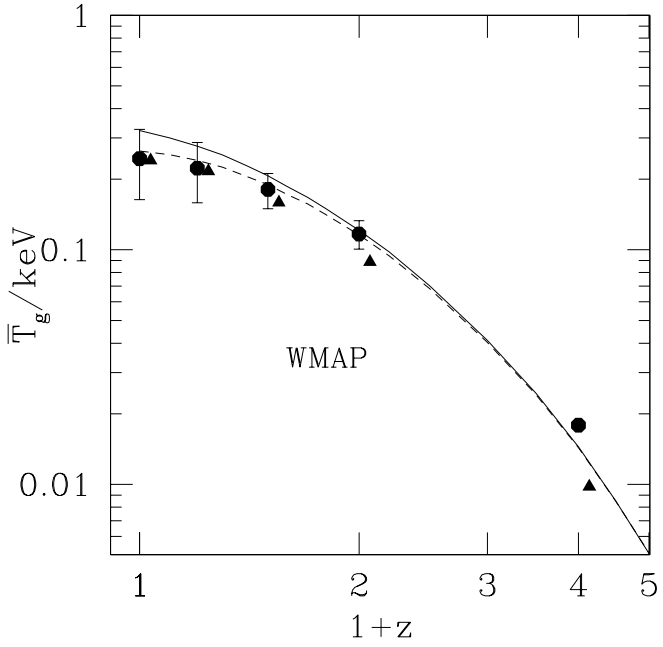

Figure 8. The resolution effect of simulations to $\bar{T}_g$. The data points with (2σ) error bars are the WMAP simulation result while the triangle data points are our model prediction using the simulated $\Delta^2_{\rm dg}$. For clarity, triangle data points are shifted horizontally arbitrarily. The solid line is our model prediction assuming gas perfectly follows dark matter and the dash line is the prediction assuming a small scale cutoff in the gas density power spectrum. The excellent agreement between two sets of data points supports the validity of our model and implies the simulation limitations to be the cause of the apparent discrepancy found in fig. 7. The excellent reproduction of the simulation results at low redshifts by the dash line implies that the simulation resolution is the cause of the discrepancy.

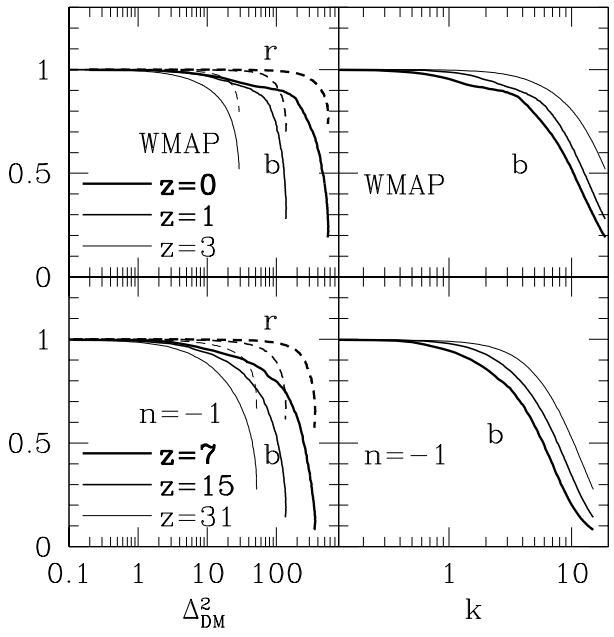

Figure 9. The gas-dark matter relation. The dash lines are the gas-dark matter cross correlation coefficients while the solid lines are the gas biases versus dark matter at different redshifts. At small nonlinear scales, gas ceases to follow dark matter in simulations. But the redshift dependence of such behavior suggests that it is unphysical and possibly caused by the simulation resolution effect. Lower redshift simulation has better mass resolution (left panel), which corresponds to better spacial resolution in unit of nonlinear scale. But spacial resolution in unit of absolute physical scale is poorer at lower z (right panel).

tion, when $k \to 0$, $f_e(k) \to r_e^2$, so the temperature bias with respect to the density field is a constant. Since gas gains thermal energy by shell crossing, which happens at the nonlinear scales, we expect r_e to be roughly equal to the density correlation length. So, the evolution of $r_e(z)$ follows that of the density correlation length. Essentially, the only free parameter in our model is $r_e(z=0)$. We will choose $r_e = r_{\rm NL}$, where r_{NL} is the non-linear scale set by $\xi_L(r_{\rm NL}) = 1$ with ξ_L as the linear correlation function. This choice of r_e has to be tested against simulations and this is the only parameter that requires calibration against simulations.

For self-similar simulations, $\Delta^2_{\rm dg}(k)$ should scales as $f(k/k_{\rm NL})$ (We define $k_{\rm NL}$ as $k_{\rm NL} \equiv 1/r_{\rm NL}$), then Eq. 8 naturally predicts

$$\bar{T}_g(z) = \bar{T}_G(z=0)(1+z)^{(n-1)/(n+3)}. \quad (9)$$

Without feedback or cooling, the gas should follow the dark matter distribution matter to very high overdensity and thus we expect $\Delta^2_{\rm dg}(k) = \Delta^2_{\rm dm}(k) = \Delta^2_g(k)$.

We calculate $\Delta^2_{\rm dm}(k)$ using the code of Smith et al. (2003). We compared the predictions from our model with simulation results and found a good agreement (Fig. 7). The scaling relation Eq. (9) with the right amplitude is observed at high redshifts and further confirms the validity of our model.

At low redshifts, the scaling relation breaks down for the self similar simulations. This is caused by the finite simulation box size. Its effect to $\bar{T}_g$ corresponds to a lower k cutoff $k_{\rm cut} = 2\pi/L$ in the integral of Eq. 8, where L is the box size. For our self similar simulations, the correlation length at $z = 0$ is half the box size and $k_{\rm NL} = 2/L$. One has $k_{\rm cut} = \pi k_{\rm NL}$. So, it is the limited box size that causes $\bar{T}_g$ in self similar simulations to lose power at low redshifts.

The deviation between the predicted and simulated $\bar{T}_g$ is also observed in the WMAP simulation. Such discrepancy increases toward low redshifts and exceeds 2σ level at $z = 0$ (Fig. 8), so it is hard to be explained by sample variance. If this discrepancy is caused by simulation limitations, $\bar{T}_g$ calculated using the simulated WMAP $\Delta^2_{\rm dg}(k)$ should agree with the simulated $\bar{T}_g$. Indeed, the agreement is better than 5% at low redshifts (Fig. 8). Thus we show that this discrepancy can be naturally explained by the simulation limitations and thus our model works well to better than several percent at low redshifts.

We further probe which simulation limitation causes this discrepancy. For WMAP simulations, even at $z = 0$, the nonlinear scale is still much smaller than the box size, so the box size effect is negligible. Resolution effect causes $\Delta^2_{\rm dg}$ to lose power at small scales and causes the simulated $\bar{T}_g$ to lose power. Since the resolution of the hydro part of

a hydro simulation is generally worse than that of the N-body part, gas ceases to follow dark matter below certain scale. Such deviation is a suitable measure of simulation resolution and can be quantified. We define the gas bias $b_g(k) \equiv \sqrt{\Delta_g^2(k)/\Delta_{\rm dm}^2(k)}$ and the gas-dark matter cross correlation coefficient $r \equiv \Delta_{\rm dg}^2(k)/\sqrt{\Delta_{\rm dm}^2(k)\Delta_g^2(k)}$. We expects $b_g(k) < 1$ at very nonlinear scales. This behavior is observed in our simulations (Fig. 9). Poorer resolution of gas with respect to dark matter means gas is smoother than dark matter, so phenomenologically, one can treat the gas density field as a smoothing of the underlying dark matter density field:

$$\delta_g(\mathbf{x}) = \int \delta_{\rm dm}(\mathbf{x}')W_g(\mathbf{x}-\mathbf{x}')d^3x'. \quad (10)$$

In this model, gas perfectly correlates with dark matter and $r \equiv 1$. In our simulation, we find that at $\Delta_{\rm dm}^2 \lesssim 200$, this is the case (Fig. 9). One can model $W_g(k) = \exp[-k^2/k_g^2]$. An ideal simulation should have a k_g such that $\Delta_g^2(k_g) \gg 1$. In simulations, $k_g(z)$ should increase with z since for higher z, the nonlinear scale is smaller (e.g. fig. 9). The simulated k_g can be modeled by $k_g(z) = 5(1+z)^2$ h/Mpc, which is roughly consistent with the simulated gas power spectrum, and reproduces the simulation results (Fig. 8). This agreement implies that for WMAP cosmology, the simulation resolution causes the simulated $\bar{T}_g$ to lose power at low redshift.

This conclusion seems counter-intuitive. Since gas temperature arises from thermalization at nonlinear scales, which are better resolved in lower redshift simulations (left panels of fig. 9 and bottom panel of fig. 10), we may expect less severe resolution problem for simulated $\bar{T}_g$ at lower redshifts. For self similar simulations, this is true since $k_{\rm NL}$ is the only relevant scale. But ΛCDM cosmology breaks self similar condition and makes the nonlinear scale $k_{\rm NL}$ not the only relevant parameter to determine $\bar{T}_g$. We show how this running power index causes more severe resolution problem for simulated $\bar{T}_g$.

The relative contribution from different scale k to $\bar{T}_g$ relies on the slope of the power spectrum. The larger the power index at $k > k_{\rm NL}$ is, the larger the relative contribution to $\bar{T}_g$ is and the higher the requirement of spacial resolution in unit of $k_{\rm NL}$ to simulate $\bar{T}_g$ is. For WMAP cosmology, $k_{\rm NL}$ keeps decreasing toward low z. The effective power index at $k = k_{\rm NL}$ keeps increasing and the relative contribution from $k > k_{\rm NL}$ keeps increasing. Such behavior requires a stronger spacial resolution in unit of $k_{\rm NL}$. In order for the simulated $\bar{T}_g$ not to lose power, at $z = 1$, simulation must be able to resolve $k \lesssim 2k_{\rm NL}$, but at $z = 0$, the requirement is $k \lesssim 10k_{\rm NL}$ (Fig. 10). As we see from the bottom panel of Fig. 10, WMAP simulation meets this requirement at $z = 1$ but fails at $z = 0$. So, we conclude that, for CDM simulation with reasonable large simulation box ($\gtrsim 50$ Mpc/h), the simulation resolution is the dominant simulation limitation to simulate $\bar{T}_g$.

In the above discussion, we have assumed that in the relevant k range, $\Delta_g^2 = \Delta_{\rm dm}^2 = \Delta_{\rm dg}^2$. Though at highly nonlinear regime, the simulated Δ_g^2 does lose power with respect to $\Delta_{\rm dm}^2$ (Fig. 9), this is likely caused by resolution effect since when increasing resolution, $b^2 = \Delta_g^2/\Delta_{\rm dm}^2$ keeps increasing toward unity (Fig. 9). Since we do not have higher resolution simulations to test if b will reach unity in these nonlinear regimes, this question still remains open. But one can estimate it using the halo model. One expects that the significant deviation from $b = 1$ could only happen where gas pressure is comparable to gravity, namely, in each halos. Observationally, intracluster gas develops a constant density core while dark matter may develop a density cusp toward the center. It is not clear whether gas pressure alone could generate such gas core or other mechanism such as feedback is required. But even the deviation in the gas and dark matter distribution presents in adiabatic simulations (with infinite resolution), it should only happen at very small scale $r \lesssim r_c \sim 0.1$ Mpc/h, or $k \gtrsim 10h$/Mpc. Thus we expect that $b = 1$ is a good approximation at scales $k \lesssim 10h$/Mpc. Since the dominant contribution to $\bar{T}_g$ for WMAP cosmology comes from $k \ll 10h$/Mpc, we do not expect the possible real deviation of b to be responsible for the discrepancy between predicted and simulated $\bar{T}_g$. We thus neglect this possible effect.

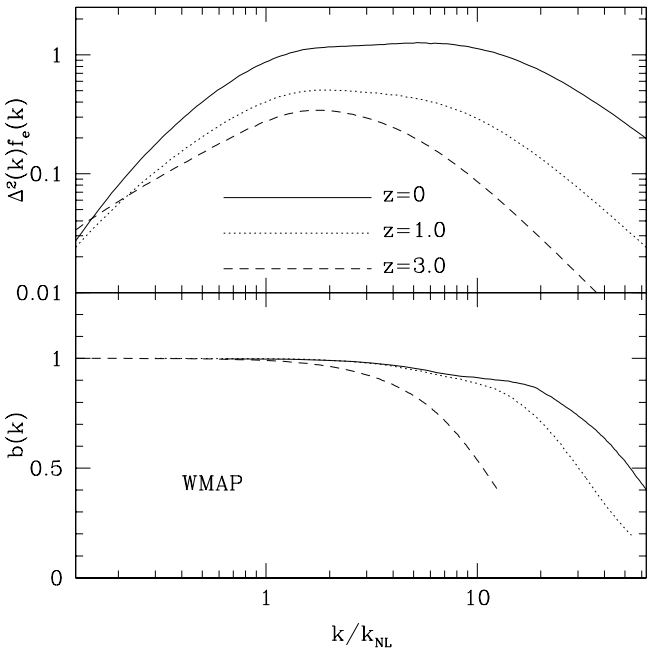

Figure 10. The requirement of $\bar{T}_g$ on simulation resolution. The top panel plots the integrand of Eq. 8, namely, the contribution of different scales to $\bar{T}_g$. The nonlinear power spectra are calculated by the Smith et al. (2003) code. At $z \gtrsim 1$, only $k \sim k_{\rm NL}$ is required to resolve. But at $z = 0$, $k \gtrsim 10k_{\rm NL}$ is required to resolve. The bottom panel is the gas bias in our simulation. Its deviation from unity is a measure of the simulation resolution. We find that, at $z \gtrsim 1$, WMAP simulation meets the resolution requirement. But at $z = 0$, the resolution requirement ($k \sim 10k_{\rm NL}$) is beyond simulation ability. Since simulated power spectrum loses power at 10% level at $k \sim 10k_{\rm NL}$, we expect the simulated $\bar{T}_g$ to lose power at 10% level, as predicted in Fig. 8.

In summary, our choice of r_e, the only free parameter in our model passes the tests of all simulations. Thus our model has no free parameter, is free of simulation artifacts and is able to predict the real $\bar{T}_g$ to several percent accuracy.

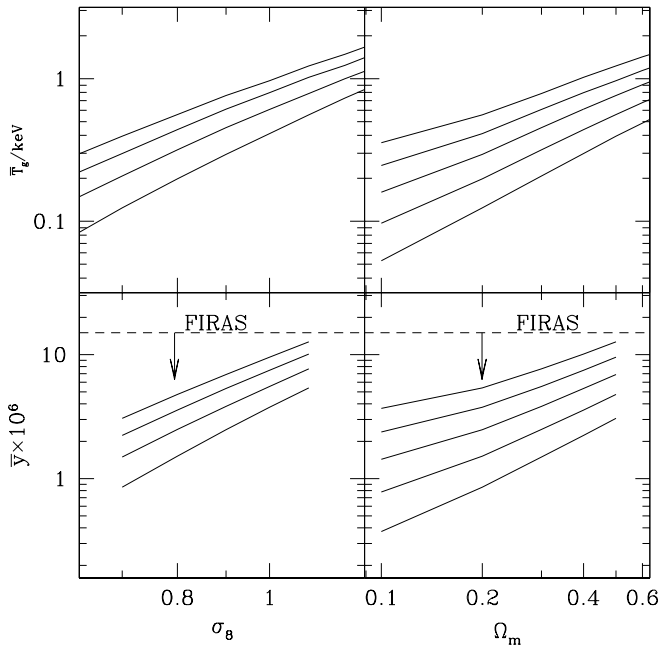

Figure 11. The predicted $\bar{T}_g$ and $\bar{y}$ as a function of σ_8 and Ω_m. For the left panels, from top down, lines correspond to $\Omega_m = 0.5, 0.4, 0.3, 0.2$. For the right panels, from top down, lines correspond to $\sigma_8 = 1.1, 1.0, 0.9, 0.8, 0.7$.

It is interesting to compare these results with the halo model prediction. For the self similar case, the same scaling relation (Eq. 9) is predicted. The scaling relation does not depend on the specific form of the halo mass function, either Press-Schechter formalism or the Jenkins fitting formula. It only relies on (1) the virial theorem $T_g \propto m^2/r_{\rm vir}$ and (2) the general form of halo mass function $dn/dm \propto m^{-2} f(\nu)|d\ln\nu/d\ln m|$. The detailed study (Refregier & Teyssier 2002) shows that the halo model prediction is consistent with simulations. Surprisingly, the halo model also tends to predict a higher $\bar{T}_g$ at low z than simulations and strongly implies the same resolution effect. The continuum model and the halo model rely on different assumptions and require different input. Though both models are based on virial theorem, the continuum model treats gas as continuum field and the halo model treats gas as distributed in discrete halos. The continuum model requires the nonlinear density power spectrum, while the halo model requires the halo mass function and the halo $m-T$ relation. The consistency in the predictions of two distinctive models gives us confidence that the predicted $\bar{T}_g$ is reliable and simulations artifacts are suitably handled.

For the WMAP cosmology, we predict $\bar{T}_g(z=0) = 0.32$ keV. $\bar{T}_g$ is sensitive to σ_8 and Ω_m. For self similar cosmology, $\bar{T}_g \propto \sigma_8^{-(n-1)/(n+3)}$. For ΛCDM, the actual dependences of $\bar{T}_g$ on σ_8 and Ω_m (fig. 11) is complicated due to the running index of the density power spectrum. In our interested σ_8 and Ω_m range, the effective power index $n_{\rm eff}$ is $-2 \lesssim n_{\rm eff} \lesssim -1$. So $\bar{T}_g \propto \sigma_8^\alpha \Omega_m^\beta$ with $\alpha \sim -(n_{\rm eff}-1)/(n_{\rm eff}+3) \sim$ 1-3 and $\beta \sim 1$. A smaller σ_8 results in a larger $k_{\rm NL}$ and thus a smaller effective power index $n_{\rm eff}$. So α is larger. The deviation of β from unity comes from the dependence of $n_{\rm eff}$ on Ω_m since CDM transfer function depends on the combination $q \simeq k/\Omega_m$. Around the WMAP cosmology $\Omega_m = 0.268$ and $\sigma_8 = 0.84$, T_g can be fitted as

$$T_g = 0.32(\sigma_8/0.84)^{3.05-0.15\Omega_m}\,(\Omega_m/0.268)^{1.28-0.2\sigma_8}\ \text{keV}. \quad (11)$$

5 THE SZ MEAN Y PARAMETER

The SZ mean y parameter is calculated using Eq. 2 and the result is shown in Fig. 11. $\bar{y}$ is generally $\sim 10^{-6}$. For the WMAP cosmology, $\bar{y} = 2.6\times10^{-6}$ and the mean temperature decrement at Rayleigh-Jeans regime is 14μK. The dominant contribution comes from $z \simeq 1$ (Fig. 12). Since at $z \gtrsim 1/2$, $d\chi/dz \propto 1/\sqrt{\Omega_m}$, one may expect $\bar{y} \propto \bar{T}_g/\sqrt{\Omega_m} \propto \Omega_m^{\sim 0.5}$. But since in a higher matter density universe, the density field evolves faster and thus $\bar{T}_g$ drops faster with increasing z, the $\bar{y}$ dependence on Ω_m is stronger than $\Omega_m^{\sim 0.5}$. Indeed, we find $\bar{y} \propto \Omega_m^{\sim 1}$. Around the WMAP cosmology $\Omega_m = 0.268$ and $\sigma_8 = 0.84$, $\bar{y}$ can be fitted as

$$\bar{y} = 2.6\times10^{-6}(\sigma_8/0.84)^{4.1-2\Omega_m}\,(\Omega_m/0.268)^{1.28-0.2\sigma_8}. \quad (12)$$

Though our model is able to predict the Compton $\bar{y}$ in an adiabatically evolving universe to several percent accuracy, it does not include any non-gravitational thermal processes, which introduce non-negligible effect to $\bar{y}$. Photoionization contributes $\bar{y}_{\rm photonion} \sim \tau 10^4{\rm K}/m_e c^2 \sim 3\times10^{-7}$, or $\sim 10\%$ of the adiabatic IGM $\bar{y}$. Though feedback, preheating, radiative cooling may decrease the SZ power spectrum by a factor of 2 (da Silva et al. 2001; Lin et al. 2002; White, Hernquist & Spingel 2002; Zhang & Wu 2003), they only affects $\bar{y}$ at 10% level (e.g. White, Hernquist & Spingel (2002)). This is straightforward to understand. Once hydrostatic equilibrium is reached, the gas pressure is always determined by the gravitational potential, which is mainly set by dark matter distribution and is only weakly affected by these thermal processes. Feedback and preheating do not change the total amount of gas. While radiative cooling turns some gas into bound objects, such mass loss is minor since bounds objects in galaxies only accounts for $\lesssim 10\%$ baryons. Thus, the change of the total gas thermal energy due to these processes is minor. These processes change $\bar{y}$ mainly during the stages of expansion in the case of feedback and preheating and infall in the case of radiative cooling. Such stages are either in semi hydrostatic equilibrium (feedback and radiative cooling) or last relatively short time (mild preheating), thus their effects to $\bar{y}$ is not significant. Cluster magnetic field also only has $\sim 10\%$ effect to $\bar{y}$ (Zhang 2004).

WMAP measured a high Thomson optical depth to the last scatter surface and implies an early reionization epoch caused by first stars. At high z, CMB density is high and is able to convert a considerable fraction of first star supernova explosion thermal energy through the efficient Compton cooling. Such first star contribution to $\bar{y}$ is $\sim$ few 10^{-6} and comparable to low redshift IGM $\bar{y}$ (Oh, Cooray & Kamionkowski 2003).

These processes have distinctive signatures to $\bar{y}$ and the SZ power spectrum, respectively. For first stars, since at high

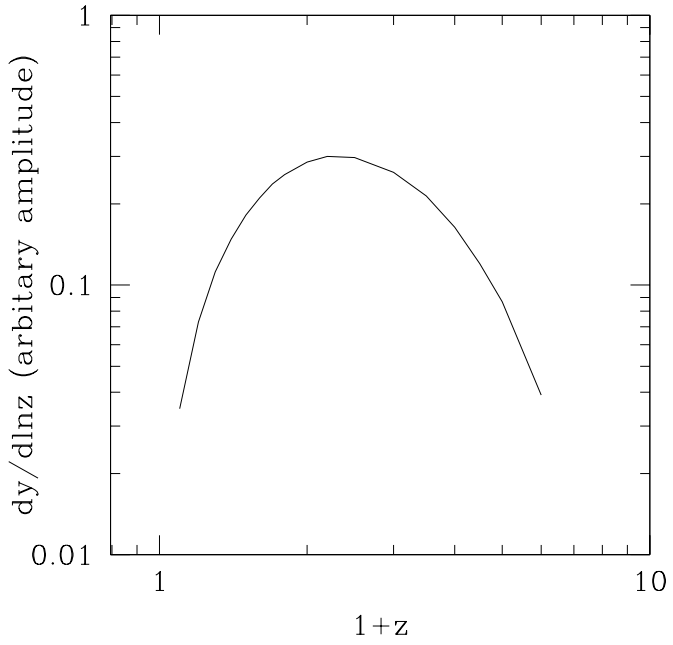

Figure 12. The integrand of $\bar{y}$, as defined by $dy/d\ln z$ for the WMAP cosmology. The dominant contribution to $\bar{y}$ comes from $z \sim 1$.

$z \sim 10$, density fluctuations are small, the relative contribution of first stars to the SZ fluctuation is much smaller than that of to $\bar{y}$. As estimated by Oh, Cooray & Kamionkowski (2003), even if first star $\bar{y}$ is larger than that of low redshift IGM, its contribution to the SZ power spectrum can still be an order of magnitude smaller than that of low redshift IGM (Fig. 1, Oh, Cooray & Kamionkowski (2003)). The case of photon-ionization is similar, but that of feedback, preheating, radiative cooling and magnetic field is opposite. Thus, combining the $\bar{y}$ and the power spectrum measurement helps to separate these contributions more unambiguously. For example, if $\bar{y}$ can be measured to $\sim 10\%$ accuracy, the first star contribution can be constrained with a statistical uncertainty $\sim 0.4 \times 10^{-6}$ and systematic underestimation of $\sim 0.5) \times 10^{-6}$ caused by feedback, etc.

Unfortunately, the direct precision measurement of absolute $\bar{y}$ is difficult. Currently, the best measurement, $\bar{y} < 1.5 \times 10^{-5}$ is given by the COBE/FIRAS measurement (Fixsen, et al. 1996). This result has already been able to rule out combinations of high $\sigma_8 \gtrsim 1.1$ and high $\Omega_m \gtrsim 0.5$. This constrain is quite weak. But considering the contributions from non-gravitational processes could make it stronger. Nonetheless, $\bar{y}$ may be measured to a higher accuracy in the future and/or inferred from new statistics and helps to independently constrain σ_8 and Ω_m.

6 SUMMARY

The mean gas density weighted temperature $\bar{T}_g$ and the mean SZ Compton y parameter are the lowest order SZ statistics. Their precision modeling stands as the first step toward the precision understanding of the IGM SZ effect and may provide useful clues for modeling of higher order statistics. The two ways of the SZ modeling, analytical models and hydro simulations both have their own limitations. It is essential to quantify simulations limitations and test analytical models against corrected simulations. The convergence of $\bar{T}_g$ stands as the lowest requirement for simulations to reliably predict the SZ effect.

We ran $n = -1, -2$ self similar 512^3 hydro simulations to quantify simulation limitations utilizing their self similar scaling relation. We also ran a high resolution 1024^3 cell, 100 Mpc/h box size hydro simulation adopting WMAP cosmology. We find that the simulated $p(> T)$, the fraction of mass with temperature bigger than T, shows a good convergence for all our simulations, except at both tails. This convergence suggests that $\bar{T}_g$ is well simulated. Our continuum field model is then tested against these simulations. It passed all tests and we believe that its prediction for $\bar{y}$ is accurate to several percent.

Various simulation limitations such as limited box size and limited resolution can affect the simulated $\bar{T}_g$. Generally, for a ΛCDM simulation, the nonlinear scale is much smaller than the box size, thus the box size effect is negligible and the resolution effect is the dominant cause of simulation artifacts in $\bar{T}_g$. Due to curvature in the CDM power spectrum, the temperature is more difficult to model accurately in simulations at fixed comoving resolution. We found that, at $z = 0$, due to the simulation resolution, gas power spectrum loses power at small scales with respect to dark matter power spectrum. This behavior causes the simulated gas density weighted temperature $\bar{T}_g$ to be $\sim 20\%$ underestimated. But this resolution effect becomes negligible quickly toward higher redshift. At $z \gtrsim 0.5$, simulated $\bar{T}_g$ is quite accurate. Since the dominant contribution to $\bar{y}$ comes from $z \sim 1$, our simulation prediction of $\bar{y}$ is reliable to $\sim 10\%$ level. Furthermore, our analytical model is able to correct this simulation artifacts and predicts $\bar{y}$ with several percent accuracy. For a flat, low matter density ΛCDM universe, $\bar{y} = 2.6 \times 10^{-6} (\sigma_8/0.84)^{4.1-2\Omega_m} (\Omega_m/0.268)^{1.28-0.2\sigma_8}$. The current upper limit of $y < 1.5 \times 10^{-5}$ measured by FIRAS has already ruled out combinations of high $\sigma_8 \gtrsim 1.1$ and high $\Omega_m \gtrsim 0.5$.

Our simulations confirms previously found $T \propto \rho$ relation in a large region of ρ-T plane. Simulation resolution may be partly responsible for this relation. But the results of self similar simulations show robust convergence of this relation and can not be explained by simulation resolution artifacts. This issue deserves a further investigation. We also found that, the simulated $p(> T, > \delta)$, does not converge. At high density regions, it is caused by density resolution limitation while at low density regions, it is caused by failure of capturing shocks. Though this numerical limitation has only minor effect on $\bar{T}_g$, it may affect the gas pressure power spectrum a lot. This issue will be addressed in a companion paper.

ACKNOWLEDGMENTS

We thank the anonymous referee for many helpful comments, especially the comparison with the halo model. Computations were performed on the CITA Pscinet computers funded by the Canada Foundation for Innovation. P.J.

Zhang is supported by the DOE and the NASA grant NAG 5-10842 at Fermilab.

REFERENCES

Atrio-Barandela, F.; Mucket, J. P., 1999, Astrophys. J., 515, 465

Bernardeau, F.; Colombi, S.; Gaztanaga, E.; Scoccimarro, R.; 2002, Phisics Reports, 367, 1

Bond, J.R.; Contaldi, C.R.; Pen, U.L.; Pogosyan, D.; Prunet, S.; Ruetalo, M.I.; Wadsley, J.W.; Zhang, P.J.; Mason, B.S.; et al., 2002, submitted to Astrophys. J., astro-ph/0205386

Cole, Shaun; Kaiser, Nick, 1988, Mon. Not. R. Astron. Soc., 233, 637

Cooray, Asantha; Hu, Wayne; Tegmark, Max; 2000, Astrophys. J., 540, 1

da Silva, Antonio C.; Barbosa, Domingos; Liddle, Andrew R.; Thomas, Peter A., 2000, Mon. Not. R. Astron. Soc., 317, 37

da Silva, Antonio C.; Kay, Scott T.; Liddle, Andrew R.; Thomas, Peter A.; Pearce, Frazer R.; Barbosa, Domingos; 2001, Astrophys. J., 561, 15L

Dave, Romeel; Cen, Renyue; Ostriker, Jeremiah P.; Bryan, Greg L.; Hernquist, Lars; Katz, Neal; Weinberg, David H.; Norman, Michael L.; O'Shea, Brian; 2001, Astrophys. J., 552, 473

Dawson, K. S.; Holzapfel, W. L.; Carlstrom, J. E.; Joy, M.; LaRoque, S. J.; Miller, A. D.; Nagai, D; 2002, Astrophys. J., 581, 86

Eke, V.; Cole, S.; Frenk, C.; 1996, Mon. Not. R. Astron. Soc., 282, 263

Fixsen, D.J., et al., 1996, Astrophys. J., 473, 576

R. W. Hockney and J. W. Eastwood, 1988, Computer Simulation Using Particles (Philadelphia: IOP).

Jenkins, A.; Frenk, C. S.; White, S. D. M.; Colberg, J. M.; Cole, S.; Evrard, A. E.; Couchman, H. M. P.; Yoshida, N., 2001, Mon. Not. R. Astron. Soc., 321, 372

Kang, Hyesung; Ostriker, Jeremiah P.; Cen, Renyue; Ryu, Dongsu; Hernquist, Lars; Evrard, August E.; Bryan, Greg L.; Norman, Michael L., 1994, Astrophys. J., 430, 83

Komatsu, Eiichiro; Kitayama, Tetsu, 1999, Astrophys. J., 526, L1

Komatsu, E. & Seljak, U., 2001, Mon. Not. R. Astron. Soc., 327, 1353

Komatsu, E.; Seljak, U., 2002, Mon. Not. R. Astron. Soc., 336, 1256

Kuo, C.L.; Ade, P.A.R.; Bock, J.J.; Cantalupo, C.; Daub, M.D.; Goldstein, J.; Holzapfel, W.L.; Lange,A.E.; Lueker,M.; et al., 2002, submitted to Astrophys. J., astro-ph/0212289

Lin,Kai-Yang; Lin, Lihwai; Woo, Tak-Pong; Tseng, Yao-Hua; Chiueh, Tzihong; 2002, submitted to ApJL, astro-ph/0210323

Majumdar, Subhabrata, 2001, Astrophys. J., 555, L7

Makino, N.; Suto, Y., 1993, Astrophys. J., 405, 1

Mason, B. S.; Pearson, T. J.; Readhead, A. C. S.; Shepherd, M. C.; Sievers, J.; Udomprasert, P. S.; Cartwright, J. K.; Farmer, A. J.; Padin, S.; Myers, S. T.; et al., 2003, Astrophys. J., 591, 540

Molnar, S. M.; Birkinshaw, M., 2000, Astrophys. J., 537, 542

Oh, S.Peng; Cooray, A. & Kamionkowski, M., 2003, Mon. Not. R. Astron. Soc., 342, L20.

Pen, U.-L., 1998, ApJS, 115, 19

Pen, U.-L., 1998, Astrophys. J., 498, 60

Press, William H.; Schechter, Paul, 1974, Astrophys. J., 187, 425

Refregier, Alexandre; Komatsu, Eiichiro; Spergel, David N.; Pen, Ue-Li, 2000, Phys. Rev. D, 6113001

Refregier, Alexandre; Teyssier, Romain; 2002, PRD, 66, 043002

Seljak, U. & Zaldarriaga, M., 1996, ApJ, 437

Seljak, Uros; Burwell, Juan; Pen, Ue-Li, 2001, Phys. Rev. D, 63, 063001

R.E. Smith, J.A. Peacock, A. Jenkins, S.D.M. White, C.S. Frenk, F.R. Pearce, P.A. Thomas, G. Efstathiou and H.M.P. Couchmann, The Virgo Consortium, 2003, Mon. Not. R. Astron. Soc., 341, 1311

Spergel, D.N.; Verde, L.; Peiris, H.V.; Komatsu, E.; Nolta, M.R.; Bennett, C.L.; Halpern, M.; Hinshaw, G.; Jarosik, N.l; et al. 2003, ApJS, 148, 175

Springel, Volker; White, Martin; Hernquist, Lars, 2001, Astrophys. J., 549, 681

Trac, H. & Pen, U.L., 2003a, PASP, 115, 303

Trac, H. & Pen, U.L., 2003b, astro-ph/0309599

White, Martin; Hernquist, Lars; Springel, Volker, 2002, Astrophys. J., 577, 569L

Zeldovich, Y.B.; Sunyaev, R., 1969, Ap&SS, 4, 301

Zhang, Pengjie; Pen, Ue-Li, 2001, Astrophys. J., 549, 18

Zhang, Pengjie; Pen,Ue-Li; Wang, Benjamin, 2002, Astrophys. J., 577, 555

Zhang, Pengjie; Pen, Ue-Li; Trac, Hy; 2004, Mon. Not. R. Astron. Soc., 347, 1224

Zhang, Pengjie. 2004, Mon. Not. R. Astron. Soc., 348, 1348

Zhang, Yu-Ying; Wu, Xiang-Ping, 2003, Astrophys. J., 583, 529